ACS OMEGA

Open Access

This article is licensed under CC-BY-NC-ND 4.0

http://pubs.acs.org/journal/acsodf

Article

Valorization of Crab Shells as Potential Sorbent Materials for CO_2 Capture

Daniel Pereira, Marina Ilkaeva, Francisco Vicente, Ricardo Vieira, Mariana Sardo, Mirtha A. O. Lourenço,* Armando Silvestre, Ildefonso Marin-Montesinos,* and Luís Mafra*

Cite This: *ACS Omega* 2024, 9, 17956−17965

Read Online

ACCESS | Metrics & More | Article Recommendations | Supporting Information

ABSTRACT: This study delves into the potential advantage of utilizing crab shells as sustainable solid adsorbents for CO_2 capture, offering an environmentally friendly alternative to conventional porous adsorbents, such as zeolites, silicas, metal−organic frameworks (MOFs), and porous carbons. The investigation focuses on crab shell waste, which exhibits inherent natural porosity and N-bearing groups, making them promising candidates for CO_2 physisorption and chemisorption applications. Selective deproteinization and demineralization treatments were used to enhance textural properties while preserving the natural porous structure of the crab shells. The impact of deproteinization and demineralization treatments on CO_2 adsorption and speciation at the atomic scale, via solid-state NMR, and correlated findings with textural properties and biomass composition were investigated. The best-performing sample exhibits a surface area of 36 m^2/g and a CO_2 adsorption capacity of 0.31 mmol/g at 1 bar and 298 K, representing gains of ∼3.5 and 2, respectively, compared to the pristine crab shell. These results underline the potential of fishing industry wastes as a cost-effective, renewable, and eco-friendly source to produce functional porous adsorbents.

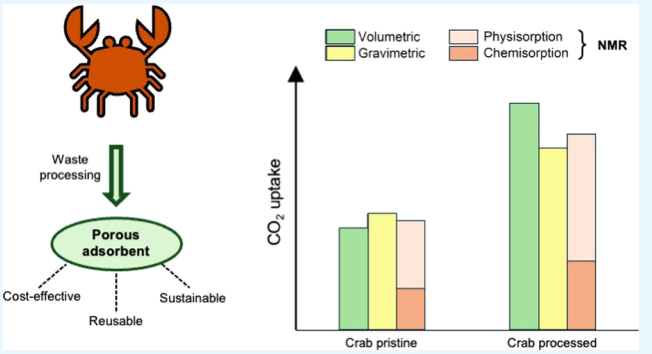

Downloaded via 156.35.62.11 on April 2, 2025 at 10:49:55 (UTC).
See https://pubs.acs.org/sharingguidelines for options on how to legitimately share published articles.

1. INTRODUCTION

Human activities such as transportation, energy production, industry, and agriculture contribute to increasing greenhouse gas (GHG) emissions, thereby trapping heat in the atmosphere. Anthropogenic GHG emissions, mainly carbon dioxide (CO_2), methane (CH_4), and nitrous oxide (N_2O) have risen significantly, with CO_2 levels starting from less than 280 ppm since the preindustrial era and surpassing 414 ppm in 2021.[1]

Various strategies have been proposed to mitigate these effects, including carbon capture and storage (CCS) technologies, which aim to capture CO_2 either directly from the air or from point sources such as power plants or cement industries, followed by its controlled storage for long periods.[2−4] The use of solid sorbents has been claimed as a promising approach to reducing CO_2 emissions due to their lower regeneration energy requirements and durability over many cycles compared with liquid amine scrubbers.[5,6]

Several materials, including metal−organic frameworks (MOFs), zeolites, silicas, porous carbons, and graphene, have been proposed as potential CO_2 capture candidates.[7−10] However, they exhibit low to moderate CO_2 adsorption capacity in their pristine form and often require costly chemical modifications with amine functionalities to enhance their CO_2 capture performance. Most of the best-performing solid adsorbents are often too costly for large-scale applications due to precursor costs or low synthesis yields. Many other materials lack suitability for large-scale use due to stability, kinetics, or regenerability issues.[6] Recently, researchers started focusing on the development of porous solid adsorbents from sustainable sources, primarily biomass processing byproducts, that are often discarded.[11] Despite offering advantages like cost-effectiveness and renewability,[12] these materials have the potential to be used in a wide range of applications,[13] including CO_2 capture.[14]

The investigation into sustainable solid CO_2 adsorbents derived from biomass waste is an emerging field, with fewer than one hundred references in the existing literature. The vast majority of the studies reported so far (∼95%) are based on the production of carbonaceous materials via thermal decomposition techniques.[15−23] Although porous carbons are popular CO_2 adsorbents[24,25] due to their rich textural properties (e.g., high surface area and extensive microporous

Received: November 26, 2023
Revised: March 16, 2024
Accepted: March 18, 2024
Published: April 12, 2024

© 2024 The Authors. Published by American Chemical Society

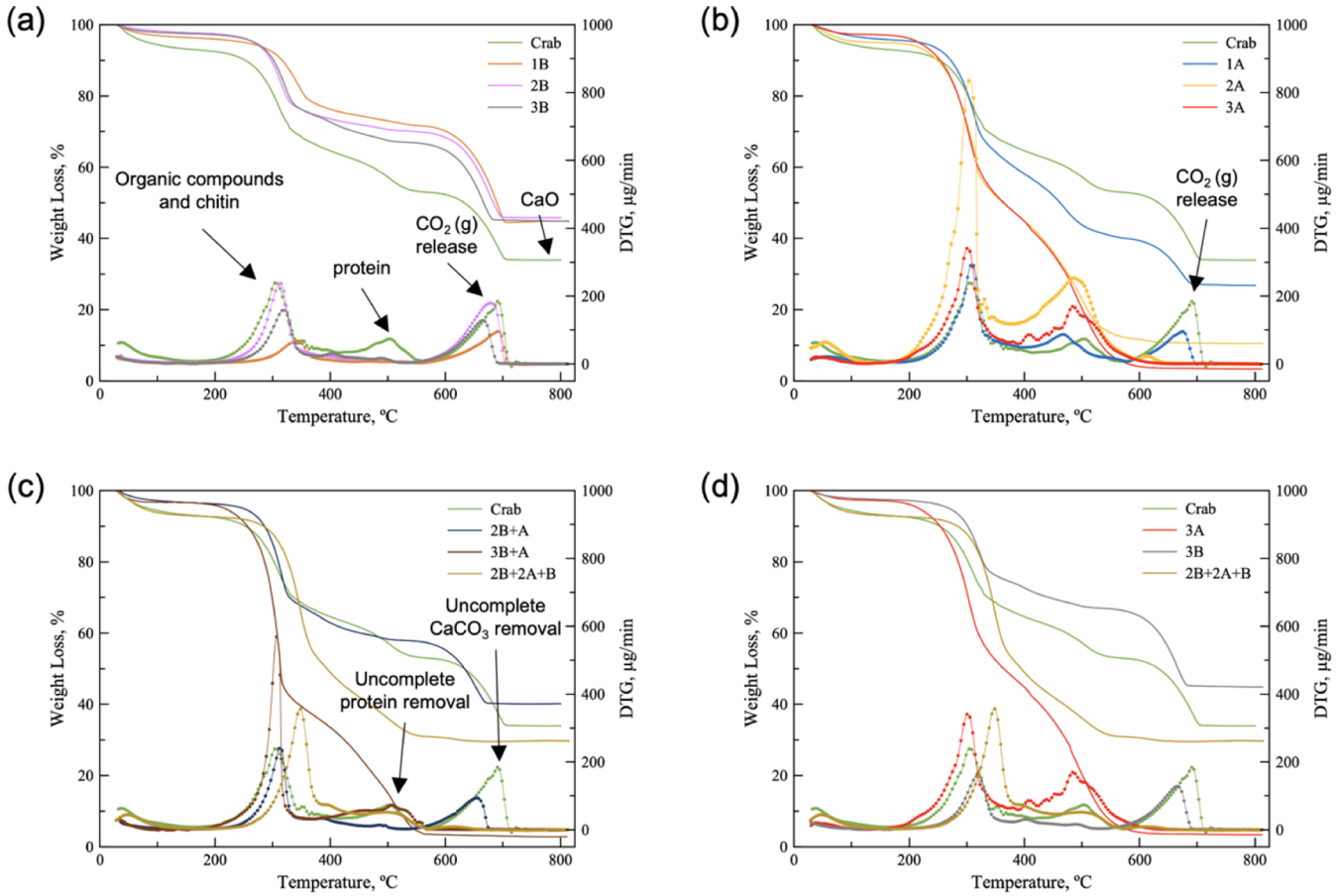

Figure 1. Comparison between the TGA curves of crab samples resulting from (a) different alkali treatments (Crab_2B and Crab_3B); (b) different acid treatments (Crab_1A, Crab_2A, and Crab_3A); and (c and d) different combination of both alkali and acid solutions (Crab_2B+A, Crab_3B+A, and Crab_2B+2A+B). In all cases, the TG curve of pristine crab shell sample (Crab) is used as a reference.

network), they frequently exhibit limited selectivity, and their production raises environmental concerns due to the energy-intensive nature of thermal decomposition methods.[24] In addition, the production of these materials suffers from low yields (~20−30%) and contributes to greenhouse gas emissions. These methods often destroy the intrinsic properties and hierarchical structure of the biomass. Apart from carbonaceous materials, some researchers have also used biomass wastes as precursors to produce mesoporous silicas for CO_2 adsorption.[26] However, the current rationale for the utilization thereof is centered on thermal decomposition methods.

In fact, recent publications have shown that biomass wastes can be used as solid adsorbents for removing pollutants from water by performing mild chemical modifications and taking advantage of their natural properties.[27,28] This type of utilization of biomass resources can also be amenable to carbon capture, as it is environmentally advantageous because it lowers processing costs and reduces carbon emissions arising from thermal decomposition methods.

The distinct inherent composition and structural properties of crustacean exoskeleton wastes make them an attractive raw material to produce solid CO_2-adsorbents. Specifically, the waste derived from Polybius henslowii crab shells was chosen for its versatile natural composition, which mainly includes chitin, proteins, calcite, and pigments, as well as its porous three-dimensional (3D)-nanoarchitecture.[29] This waste stream is particularly appealing for CO_2 capture applications because of its natural porosity and N-bearing groups natively present in its structure.[6,30−32] Additionally, crab shell waste is produced in large quantities, with close to 370,000 tons generated in EU-28 in 2016 from just one species of crab.[33] These residues are generally either harvested for chitin/chitosan production or landfilled/incinerated at a large-scale, which can be leveraged to produce low-cost CO_2-adsorbents. Repurposing biomass wastes into CO_2-adsorbent materials prevents their incineration and the resulting CO_2 emissions, thereby aligning with the principles of a sustainable circular bioeconomy.

Herein, we use crab shells as biomass waste to develop a low-cost and eco-friendly CO_2 adsorbent by applying strategic deproteinization and demineralization treatments aiming to enhance its natural porosity. The impact of these chemical treatments on adsorption performance and CO_2 speciation was investigated at the atomic scale using solid-state NMR, whose results were correlated to textural properties and biomass composition of the prepared sorbents to obtain structure−property relationships.

2. MATERIALS AND METHODS

2.1. Chemicals. NaOH (Honeywell, >98%), HCl (Fluka, 37 wt %), chitin (TCI), and $CaCO_3$ (TCI) were used as received.

2.2. Sorbents Preparation. Discarded crabs, with ~5 cm, were collected from Mira beach, Portugal, and boiled at 90 °C for 20 min. After being cooled, the crab flesh was separated

https://doi.org/10.1021/acsomega.3c09423
ACS Omega 2024, 9, 17956−17965

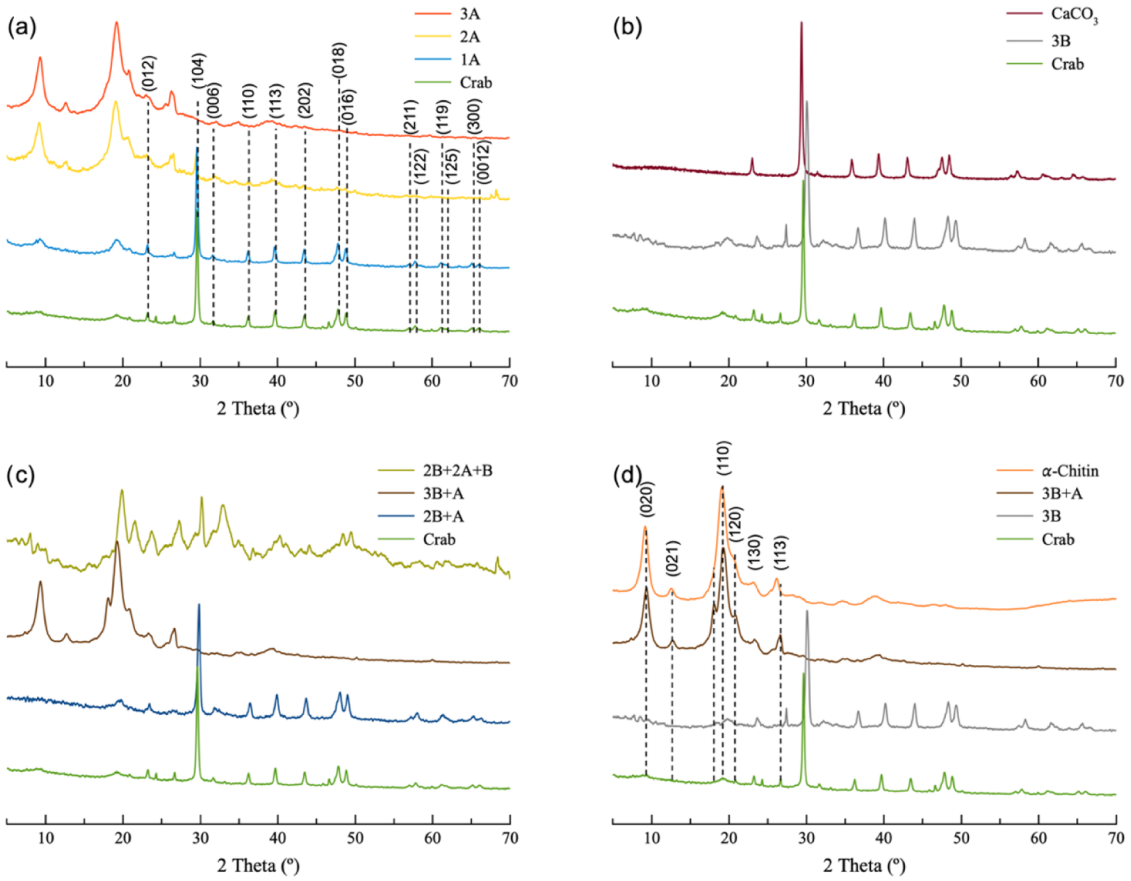

Figure 2. PXRD of (a) crab samples treated with acid solution; dashed lines represent the diffraction planes of calcite; (b) crab samples treated with alkali solution; (c) crab samples treated with both alkali and acid solutions; and (d) comparison between crab, crab sample treated with three consecutive alkali treatments, and crab sample treated with three consecutive alkali treatments followed by an acid treatment; dashed lines denote the diffraction planes of chitin. B denotes for alkali-treated samples and A stands for acid-treated samples.

from the shell, and the latter was frozen at −18 °C until further use. Then, 63 g of the different parts of the crab shell (carapace, claw, and crawling legs) were blended in 63 mL of distilled water for 2 min using a blender machine (Braun, 300 W). The blended crab shell was filtered off, washed with 50 mL of distilled water, and dried overnight at 60 °C in an oven. The obtained crab shell material (thereafter named Crab) was crushed with the help of a pestle and mortar.

To fine-tune the crab shell porous structure toward enhanced natural porosity and improved CO_2 capture properties, conventional chemical treatments have been applied to selectively remove partially/completely proteins and minerals. The treatments performed in this work are adapted from the literature based on the conventional two-step process for chitin nanofiber extraction from crab shells.[34]

Deproteinization was carried out by mixing 5 g of crab sample with 30 mL of NaOH solution (1 M) and stirring overnight at room temperature. The obtained solid was filtered, washed with distilled water until neutral pH, and dried at 60 °C to prepare Crab_*n*B samples, where *n* represents the number of treatments and B denotes alkali treatment. Consecutive basic treatments were performed until no significant changes were observed in the protein content of the deproteinized samples.

The demineralization, mainly used for $CaCO_3$ removal, was carried out by stirring 5 g of crab sample with 30 mL of diluted aqueous HCl (1 M) at room temperature for 24 h. Analogous to the procedure used for the deproteinization, the acid treatment was iteratively repeated for *n* consecutive cycles until all of the $CaCO_3$ was removed. Samples were labeled as Crab_*n*A samples, where *n* represents the number of treatments and A denotes acid treatment.

Different combinations of the deproteinization and demineralization processes (alkali and acid treatments, respectively) were performed to obtain porous chitin-based solids following the procedures previously described. The obtained yields for each sample are presented in Table S1.

2.3. Sorbents Characterization. The samples prepared in this study were characterized by Fourier transform infrared (FTIR) spectroscopy, powder X-ray diffraction (PXRD), scanning electronic microscopy (SEM), thermogravimetric analysis (TGA), elemental analysis (EA), low-temperature (77 K) nitrogen adsorption−desorption isotherms, 298 K CO_2 adsorption isotherms, and solid-state nuclear magnetic resonance (SSNMR) spectroscopy. The equipment and experimental parameters used are described in Supporting Information (SI).

3. RESULTS AND DISCUSSION

3.1. Tailoring the Porosity of Crab Shell toward Improved CO_2 Adsorption. Crab shells are mainly composed of chitin, protein, and $CaCO_3$. These components are arranged within a 3D nanostructure conferring natural porosity to crab shells, which can be fine-tuned by extracting some of these components.[35] Chitin is surrounded by proteins

https://doi.org/10.1021/acsomega.3c09423
ACS Omega 2024, 9, 17956−17965

forming bounded chitin−protein fibers organized in a Bouligand-type structure.[36,37] The present study aims at producing porous nanofibril chitin materials by treating crab shells with alkali and acid solutions to selectively remove, partially or completely, the protein and $CaCO_3$ components.

TGA was used to quantify the content of organic compounds (proteins and chitin) and minerals (calcite) in the samples (Figure 1 and Table S2). Based on this technique, considering the weight losses at the typical decomposition temperatures of each component, the most abundant component of the crab shell is $CaCO_3$ (42.8 wt %), followed by chitin (24 wt %) and protein (10.7 wt %). These values agree with the published data for this material.[36] While other minerals may be present in crab shells, as confirmed by scanning electron microscopy/energy-dispersive spectroscopy (SEM/EDS) analysis (Figure S1 and Table S3), the residual quantity of minerals detected at 800 °C (typically associated with CaO) was not taken into consideration for determining the amount of $CaCO_3$. Instead, the calculation relied on the measurement of the quantity of CO_2 gas released during the decarboxylation process of $CaCO_3$, which typically occurs between 600 and 750 °C (Figure 1).[38,39]

The thermal degradation of crab samples occurs in four main steps. The first weight loss (below 150 °C) is related to the dehydration process and the release of other volatile compounds.[38,39] The second weight loss is attributed to chitin depolymerization and destruction, which typically degrades between 250 and 400 °C.[38,39] The third weight loss, between 450 and 550 °C, is associated with protein thermal degradation. Finally, the fourth weight loss is related to the thermal decomposition of $CaCO_3$ into CaO and CO_2.[38,39] Thus, the absence of the last two weight losses on treated samples confirms the deproteinization (Figure 1a) and demineralization (Figure 1b) of the crab sample. This last process is only fully achieved after three consecutive acid treatments (Crab_3A sample). When both acid and alkali treatments are performed, the relative amount of chitin in the resulting samples increases, while protein and $CaCO_3$ contents decrease (Figure 1c and Table S2). TGA of the sample Crab_3B+A indicates the presence of chitin and protein (Figure 1c and Table S2), showing that the mild conditions used to remove proteins from the crab shell are inefficient in eliminating this component even after three consecutive alkali washing cycles.

PXRD patterns were recorded to further confirm the composition of the crab sample before and after treatment (Figure 2). In our study, PXRD was particularly useful to identify the presence of $CaCO_3$ and chitin in various crab-derived samples. The removal of $CaCO_3$ is observed in the diffraction patterns of calcite (ICDD database code: 04-006-6528) in Figure 2a after three consecutive acid treatments. However, if deproteinization of the crab shell is performed first through three consecutive alkali treatments, a single acid wash is enough to remove $CaCO_3$ (Figure 2c,d, Crab_3B+A sample). This result is due to the enhanced porosity of the crab shell structure, which allows the aqueous acid solution to easily diffuse across the porous network of the shells, leading to a more efficient extraction of $CaCO_3$. This sample (Crab_3B +A) displays almost pure α-chitin (ICDD database code: 00-035-1974), identified through the diffraction peaks at 2θ = 9.6, 18.6, 19.4, 21.0, 23.6, and 26.8°[40,41] (Figure 2d) while sample Crab_2B+2A+B still contains some $CaCO_3$, highlighted by the calcite diffraction plane (104) at 29.6° (Figure 2c), despite undergoing similar number of alkali treatments, with one additional acid treatment. This indicates that the order in which the treatments are performed affects the final properties of the resulting materials. FTIR spectroscopy was also performed to analyze the components of the crab-based samples (Figure S2), providing complementary data for the unambiguous interpretation of the contributions of acid and alkali treatments. Deproteinization treatment allows the identification of a split peak in the amide vibrational models (at ∼1630 cm^{-1}),[42] which can be attributed to the presence of the chitin α-polymorph.[43] The IR bands corresponding to $CaCO_3$[44] (at 1789, 1460, and 870 cm^{-1}) persist after 3 alkali treatments, albeit vanishing after 3 acid treatments (further discussion in the SI). Overall, the PXRD and FTIR analysis corroborates the previous observations derived from TGA, elucidating the acid and alkali treatments' contributions to crab shell composition. Acid treatments efficiently demineralize the shells, whereas alkali treatments are optimal for deproteinization.

SEM (Figure S1) and SEM/EDS (Table S3) techniques were employed to examine the surface morphology and elemental composition of crab and crab-derived samples. The analysis revealed a prominent presence of C, Ca, and O elements in the crab shell, indicating the existence of $CaCO_3$ on its surface (Table S3 and Figure S1A,B). Treatment of the materials with acidic and alkali aqueous solutions induced significant composition and textural changes in the crab surface (Figure S1 and Table S3). Following three acid treatments, Ca was depleted, O decreased by 5.19 wt %, while C and N increased by 12.24 and 4.25 wt %, respectively. These results confirmed the complete extraction of $CaCO_3$ from the crab, thereby exposing α-chitin as observed in the XRD data. Furthermore, the $CaCO_3$ removal allowed the detection of F and Si elements (Table S3), with the latter possibly originating from a small quantity of sand present in the crab shell. The acid treatment appeared to enhance the macroporosity, as evidenced by the observation of layers of chitin−protein fiber complexes (Figure S1C). SEM images of the Crab_3B sample show a disorganized macropore structure (Figure S1D). EDS analysis indicates a significant reduction of the C (approximately half of the pristine crab sample) and N elements, along with a nearly 2-fold increase in Ca content, confirming the protein extraction. When this sample was treated with dilute HCl, $CaCO_3$ seemed to be efficiently removed in a single treatment, as it was not detected by SEM/EDS analysis (Table S3). The removal of a significant portion of protein and $CaCO_3$ appeared to lead to the collapse of the crab shell's pore structure, resulting in a dense chitin nanofiber arrangement (Figure S1E). A similar behavior was observed by Gbenebor et al.[45] during the deproteinization and demineralization of shrimp shells. A different result is observed in the Crab_2B +2A+B sample. In this case, despite the crab shell being treated three times with an alkaline solution and twice with an acid solution, a small amount of protein and $CaCO_3$ remained in the sample (Table S3). The presence of these components prevented the complete collapse of the natural pore structure of the crab shell (Figure S1F), highlighting that the order of treatments affects the sample textural properties. This behavior is advantageous for adsorption applications, as demonstrated by Synowiecki and Al-Khateeb,[46] who showed that the number of pores on the chitin surface is related to its capacity to absorb metal ions, which is enhanced with increased porosity. Complementary results were obtained from CHNS elemental

https://doi.org/10.1021/acsomega.3c09423
ACS Omega 2024, 9, 17956−17965

analysis (Table S4), where increasing the number of treatments with acid solution enhanced the C and N percentages in the resulting crab samples, confirming the extraction of calcite and corroboration of the SEM/EDS and TGA results. The opposite is observed when alkali treatments are performed. In this case, the C and N percentages decrease, and the amount of minerals (observed as the difference of CNH relative quantities) is enhanced.

To further explore the textural properties of the crab-based materials, low-temperature N_2 volumetric gas adsorption measurements were performed in a selection of samples which represent different combinations of components (i.e., chitin, protein, and $CaCO_3$) in the crab-derived materials. The surface areas, calculated from N_2 adsorption isotherms, are summarized in Table 1. All samples exhibit a type IIb isotherm with an H3 hysteresis loop (Figure 3a), except for Crab_3A, which showed negligible adsorption of N_2. The pristine sample, Crab, exhibits a surface area value of 10 m^2/g, consistent with findings from other studies on waste-based materials derived from crustaceans.[47,48] As discussed in the previous sections, the textural properties of the crab-based materials could be tailored by employing acid, alkali, or combined treatments. Solely applying acid treatment (e.g., Crab_3A) led to extremely low N_2 adsorption owing to the removal of the $CaCO_3$ fraction from the material, resulting in the collapse of the naturally porous structure of the crab shell. Conversely, the removal of the proteic part during the alkali treatment steps enhanced the surface area, reaching maximum values for Crab_2B+2A+B and Crab_3B samples, with V_{total} values of 0.12 and 0.11 cm^3/g and S_{BET} values of 36 m^2/g for both. For the pore size distribution analysis, see Supporting Information (Figure S3). These findings agree with the XRD, TGA, and SEM data, suggesting that the presence of residual quantities of protein or $CaCO_3$, as well as the order in which their partial removal occurs, is critical for maintaining the materials' structural integrity. These components act as scaffolds, preventing the collapse of the natural pore structure of the crab shell.

Table 1. Overview of the Textural Properties of the Pristine Crab Shell and Crab-Derived Samples[a]

Sample[b]	S_{BET} (m^2/g)	V_{total} (cm^3/g), at p/p_0 = 0.99
Crab	10	0.07
Crab 2B+A	27	0.12
Crab 2B+2A+B	36	0.12
Crab 3B	36	0.11
Crab 3A	n/a	0.01
Crab 3B+A	6	0.03
chitin	5	0.05

[a]n/a-S_{BET} was not calculated due to the negligible adsorption of N_2 at 77 K. [b]Sample designation explained in Section 2.2.

3.2. CO_2 Adsorption Studies in Crab-Derived Solid Sorbents Using a Multitechnique Approach. This section examines the CO_2 adsorption capabilities of the studied crab shell materials exposed to various treatments. The studied compounds herein encompass the following samples: the pristine crab (Crab), demineralized sample (Crab_3A), and deproteinized sample (Crab_3B), as well as samples with partial removal of protein and $CaCO_3$ fractions (Crab_2B+A and Crab_2B+2A+B), and samples with significant removal of protein and $CaCO_3$ fractions (Crab_3B+A).

3.2.1. CO_2 Adsorption Capacity Studies. Volumetric gas adsorption measurements, CO_2 at 298 K and 1 bar, were performed to determine the maximum CO_2 uptake of the crab selected samples (Figure 3b and Table 2). The sample Crab_2B+2A+B demonstrates the highest CO_2 uptake of 0.31 mmol/g, which correlates well with the highest S_{BET} and V_{total} values (Table 1) of this series of samples. Interestingly, the pristine sample also demonstrates a significant amount of CO_2 adsorption of 0.17 mmol/g.

Table 2. CO_2 Adsorbed Quantities (mmol/g) at 25 °C and 1 bar determined using different techniques

	CO_2 uptake 1 bar, 298 K [mmol (CO_2)/g (sample)]		
Sample	Volumetric	Gravimetric	NMR
Crab	0.14	0.16	0.15 (0.09[a] + 0.06[b])
Crab_2B+A	0.13	0.14	0.17 (0.11[a] + 0.06[b])
Crab_2B+2A+B	0.31	0.25	0.27 (0.18[a] + 0.09[b])
Crab_3B	0.16	0.18	0.20 (0.14[a] + 0.06[b])
Crab_3B+A	0.14	0.11	0.11 (0.09[a] + 0.02[b])
Crab_3A	0.09	0.10	0.09 (0.09[a] + 0.00[b])

[a]Physisorbed CO_2. [b]Chemisorbed CO_2.

As previously mentioned, the CO_2 adsorption mechanisms are highly sensitive to the surface chemistry of the adsorbents. To assess the affinity of CO_2 toward the surface of the crab-derived sorbents, Henry's constants (K_H) and the viral

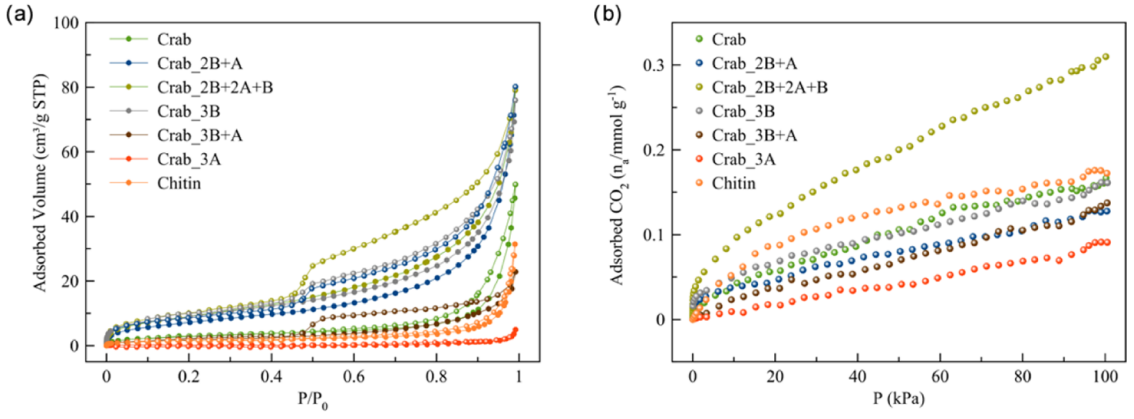

Figure 3. Adsorption−desorption isotherms of (a) N_2 and (b) CO_2 recorded at 77 and 298 K for the selected crab-derived samples.

https://doi.org/10.1021/acsomega.3c09423
ACS Omega 2024, 9, 17956−17965

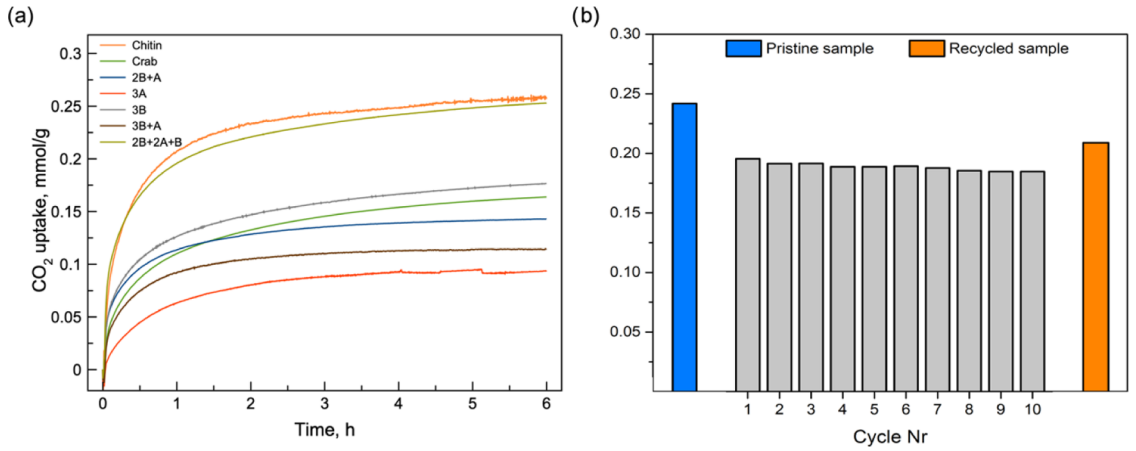

Figure 4. TGA: (a) CO_2 adsorption at 298 K, 1 bar; (b) CO_2 adsorption of sample Crab_2B+2A+B during 10 continuous adsorption/desorption cycles. The TGA mass value at times of 0 and 2 h was used to calculate the amount of CO_2 adsorbed.

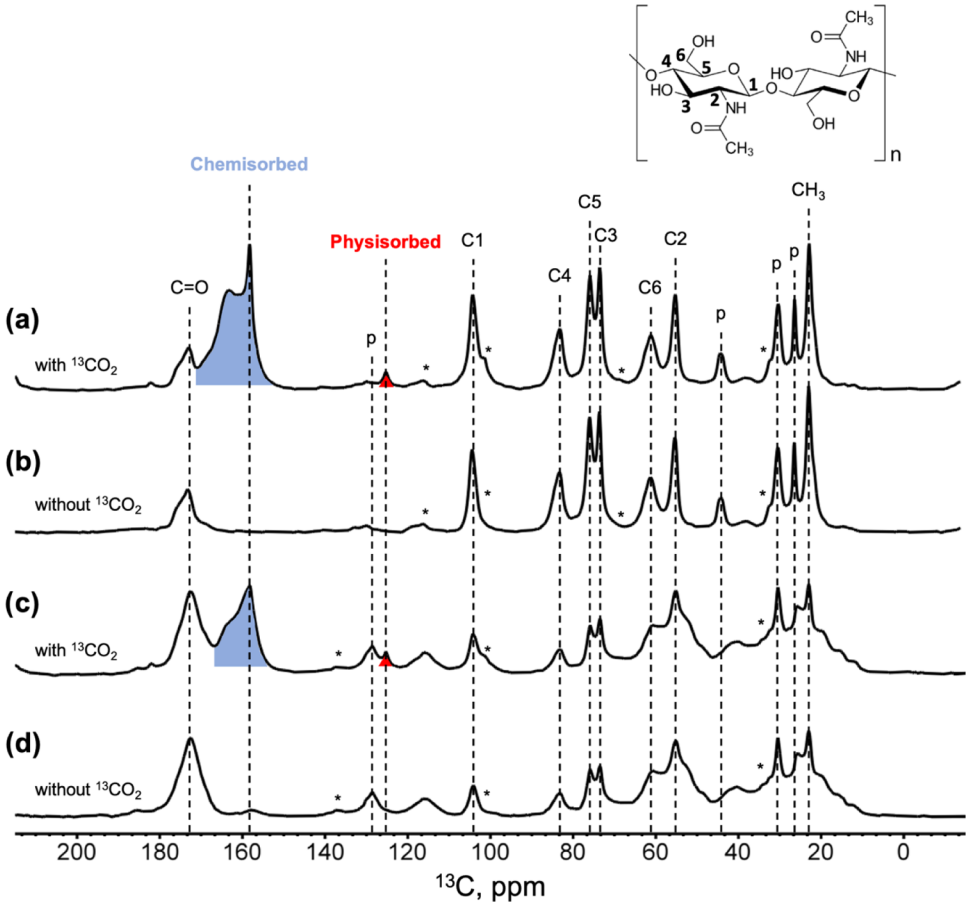

Figure 5. ^{13}C CP-MAS spectra of Crab_2B+2A+B after (a) and before (b) $^{13}CO_2$ exposure and pristine crab shells after (c) and before (d) $^{13}CO_2$ exposure. The data was recorded at a field strength of 16.4 T and a MAS speed of 10.0 kHz. The chitin peaks are identified as "C1", ⋯, "C6", and protein peaks are identified as p. Chemisorbed and physisorbed CO_2 species are highlighted as blue and red, respectively. * depict spinning sidebands.

coefficients C_1 and C_2 were calculated from the CO_2 isotherms for each sample (Figure S4 and Table S5). The highest K_H values, representing higher affinities toward CO_2, were obtained for the samples Crab_2B+2A+B, Crab_3B, and commercial chitin, whereas the lowest K_H values were observed for the Crab_3A and Crab_3B+A. The steep increase of CO_2 uptake at low pressure, at the beginning of the isotherms (Figure 3b), suggests that most likely N-bearing groups from chitin and remaining protein are participating in the CO_2 chemisorption process. Although these samples might contain residual quantities of protein, it seems that it is either too small in quantity or simply not accessible due to the collapse of the porous structure and reduction of the surface area (Table 1). Additionally, the isotherms were fitted with the Freundlich model (Figure S4 and Table S5), from which a similar adsorption trend was observed. Interestingly, the Crab_2B+2A

https://doi.org/10.1021/acsomega.3c09423
ACS Omega 2024, 9, 17956−17965

+B sorbent shows an amide efficiency (defined as the ratio of moles of CO_2 adsorbed to the moles of N present in the samples) of 0.10, almost 2.7 times higher than the one obtained for commercial chitin, suggesting improved accessibility of CO_2 to the amide groups in this sample. The improved CO_2 adsorption can be explained by increased pore diffusion or the nature of the N-bearing groups present in the crab-derived sorbent material.

3.2.2. Recyclability Studies. TG adsorption analysis was conducted to study the adsorption kinetics of pure CO_2 in the selected samples. Figure 4a shows the adsorption curve, which demonstrates that all samples require extended exposure times to saturate the adsorption sites. Table 2 presents a summary of the CO_2 uptake determined for each individual sample. The sample Crab_2B+2A+B exhibited the highest adsorption capacity among the selected samples, with a capacity of 0.25 mmol/g, consistent with the values obtained from the volumetric adsorption experiment (Table 2).

Despite the extended gas exposure times required to attain saturation of the adsorbents, the CO_2 adsorption can be optimized to replicate in-operando conditions using the adsorption kinetic profile (Figures 4a and S5). For instance, Crab_2B+2A+B exhibited rapid adsorption during the first 2 h of CO_2 exposure, followed by a gradual increase until the end of the 6 h exposure period. (Figure S5). This initial fast CO_2 adsorption results in a gas capture equivalent to 77.4 and 87.4% of the total uptake, at t = 1 and 2 h respectively, revealing an auspicious equilibrium between the amount of CO_2 adsorbed and the gas exposure duration, showing a similar behavior as commercial chitin, despite having 1/3 less N content in the sample (Table S4).

The recyclability of crab-based materials was evaluated by conducting adsorption/desorption cycles on the best-performing sample (Crab_2B+2A+B) toward CO_2 uptake. The experimental measurement was performed using 2 h of CO_2 exposure followed by a thermal degassing at 120 °C with 30 min dwell time. The adsorption/desorption cycles, presented in Figure 4b, show a progressive loss of adsorption capacity during the 10 cycles (Figure 4b, gray bar). After the 10th cycle, a long thermal degassing was performed to regenerate the sample, leading to a recovery of 83.5% of the initial adsorption capacity (Figure 4b, orange bar).

3.2.3. Quantitative Assessment of Chemi- and Physisorbed CO_2 Species by ^{13}C MAS NMR. Solid-state NMR (SSNMR) spectroscopy is a powerful site-selective technique capable of probing the local structure and dynamics of adsorbed molecules inside porous networks. In this study, SSNMR was used for the quantitative assignment of chemi- and physisorbed CO_2 species. Figure 5 shows the ^{13}C cross-polarization magic-angle spinning (CP-MAS) spectra of two materials before and after exposure to 1 bar of $^{13}CO_2$ at 298 K. The spectrum of pristine crab, (Figure 5c,d) depict distinct resonances of α-chitin carbons observed at ca. 22.2 (CH_3), 54.2 (C2), 61.1 (C6), 73.1 (C3), 75.4 (C5), 82.5 (C4), and 104 (C1) ppm, consistent with previously reported NMR data.[49] The resonances attributed to the protein domain (labeled with "p") were also identified. A broad peak comprising the protein, chitin, and $CaCO_3$ signals is observed in the carbonyl region between 165 and 190 ppm. The spectrum of the Crab_2B+2A+B sample before CO_2 adsorption (Figure 5a,b) displays comparable chitin spectra to the pristine sample, albeit with reduced protein and $CaCO_3$ contents.

Different acid and alkali treatments were strategically used to selectively remove calcium carbonate or protein to force the spectral separation between $CaCO_3$, chitin, and protein carbonyl NMR signals. Figure S6 displays MAS spectra of crab shell samples after performing three alkali treatments (Crab_3B), pristine shells, and commercial α-chitin and $CaCO_3$. Three alkali treatments remove most of the associated protein, leaving chitin and $CaCO_3$ as the major components. As a result, the signals at 173 and 169 ppm in Crab_3B spectrum correspond to chitin carbonyl and $CaCO_3$, respectively, which is consistent with previously reported values in the literature[50] and the ^{13}C signals observed in the commercial α-chitin and $CaCO_3$ spectra.

Following $^{13}CO_2$ adsorption (Figure 5), both broad and sharp signals appear within the 155−166 and 125 ppm range. The peak at 125 ppm can be unambiguously assigned to physisorbed CO_2 as reported previously.[8,51] The broad peak at 155−166 ppm appears in the chemical shift range attributed to chemisorbed CO_2, usually associated with the formation of carbamic acid and carbamate ion pair, among others, as extensively reported in previous works.[4,8,52] A detailed assignment of the different CO_2 species formed in this complex multicomponent material (chitin, protein, minerals, ···) is beyond the scope of our contribution.

NMR quantification of CO_2 adsorption was carried out by using ^{13}C direct excitation experiments. The adsorbed $^{13}CO_2$ quantity was determined by extrapolation from a calibration curve of 1−2-^{13}C-Glycine, as shown in Figure S7. The ^{13}C direct excitation spectrum used for quantification was deconvoluted and integrated, as shown in Figures S8 and S9. The quantification results are shown in Table 2, highlighting that most of the CO_2 molecules are adsorbed via a physisorption mechanism. The NMR quantification results presented are in very good agreement with the CO_2 uptake of the same samples determined by volumetric and gravimetric techniques (Table 2).

3.3. Cost Analysis of Crab-Based Adsorbents. One of the most appealing properties of crab-based adsorbents is their extremely low price. Considering the high volume of crab shells produced worldwide and the limited use of such a biomass waste stream, it is no surprise that the price of these shell wastes can be as low as 100 $ per ton of residues in wholesale suppliers. Considering the yield obtained for our best-performing sample, Crab_2B+2A+B, we determined that a ton of this adsorbent would account for a cost of around 376 $ (or ∼0.4 $/kg) (see Supporting Information for additional details). This value is incredibly low when compared to the price of other adsorbents such as UTSA-16 (∼258 $/kg), Mg-MOF-74 (∼4040 $/kg), and Zeolite 13X (∼87 $/kg). These values have been calculated using prices for bulk chemicals from common scientific suppliers and yields reported in the literature.[53] Moreover, the industrial economies of scale play an important role in driving the price of a given adsorbent orders of magnitude lower, as demonstrated by Zeolite 13X with its industrial price around 2 $/kg.[53] Similar effects should be expected for any adsorbent deployed at the industrial level.

Despite the total CO_2 uptake capacity determined for the best crab-based adsorbent is somewhat lower when compared to other values displayed for benchmark solid adsorbents across the literature, it is important to stress that this is only one factor among many others affecting the suitability of solid adsorbents for CO_2 capture applications. Such an example is displayed in the study published by Petit et al., where multiple

https://doi.org/10.1021/acsomega.3c09423
ACS Omega 2024, 9, 17956−17965

materials are compared across different stages of the CO_2 capture process and their performances are evaluated.[53] Curiously, Mg-MOF-74 exhibits a much higher isothermal amount of CO_2 adsorbed compared to that of USTA-16 MOF. Nevertheless, the high enthalpy of adsorption causes a generalized decrease in the working capacity of Mg-MOF-74, impairing its performance when compared to USTA-16. Moreover, other factors such as CO_2 purity also play a very important role in the process economics. High N_2 adsorption also affects Mg-MOF-74, further impairing its performance by reducing the purity of the CO_2 capture. This example is of paramount importance, as it clearly demonstrates that comparing CO_2 capacities is not necessarily significant. Rather, an integrated analysis considering working capacity, recovery, and working selectivity should be performed to accurately evaluate the performance and suitability of different CO_2 adsorbents. This analysis is outside the scope of this work.

4. CONCLUSIONS

This study focused on the development of a low-cost and eco-friendly CO_2 adsorbent using crab shell waste by tailoring the porosity of crab shells through deproteinization and demineralization treatments. The resulting materials were comprehensively characterized by using various analytical techniques.

A variety of treatment combinations involving acid and alkali washes were systematically conducted to control the relative proportions of the main components of the crab shells, namely, chitin, protein, and $CaCO_3$. Acid treatments were observed to be effective in the demineralization of crab shells, while alkali treatments demonstrated superior suitability for the selective removal of proteins. Pristine crabs (Crab), demineralized sample (Crab_3A), deproteinized sample (Crab_3B), as well as samples with partial removal of protein and $CaCO_3$ fractions (Crab_2B+A and Crab_2B+2A+B), and samples with significant removal of protein and $CaCO_3$ fractions (Crab_3B+A) were extensively characterized to elucidate the roles played by the individual components of crab shells and establish relationships between the shell's structural composition and adsorption properties.

The volumetric adsorption isotherms revealed that residual quantities of protein and $CaCO_3$ appear to play a valuable role in maintaining the structural integrity of the natural 3D-nanoarchitecture of crab shells. The sample with a higher surface area (Crab_2B+2A+B), 36 m^2/g, exhibited the best CO_2 uptake capacity. This sample exhibited a high K_H, indicating higher affinity toward CO_2 due to higher accessibility and availability of the amide groups to interact with the gas. TG recyclability experiments show that the Crab_2B+2A+B sample can be effectively regenerated over multiple adsorption/desorption cycles, with only a partial loss in CO_2 uptake observed. Moreover, ssNMR measurements show that CO_2 adsorption occurs via chemi- and physisorption mechanisms, with a greater amount being captured through the latter mechanism.

Overall, this study showcases the potential of transforming readily available bio-waste into an effective and economical CO_2 adsorbent, highlighting the importance of exploring unconventional sources for sustainable and impactful solutions to address the global environmental challenge. While extensive research on the role of crab shell components on the textural and adsorption properties was carried out in this work, other aspects influencing the performance of solid adsorbents should merit further studies in the future, e.g., the strength and duration of acid and alkali treatments, particle shape, and how drying methods affect the porous network of the crab adsorbents, among others.

■ ASSOCIATED CONTENT

Supporting Information

The Supporting Information is available free of charge at https://pubs.acs.org/doi/10.1021/acsomega.3c09423.

Experimental details of the analytical characterization used in this work are provided and a selection of supplementary results and discussion are also provided: yields of sample preparation; SEM images of various crab-derived samples; elemental analysis by SEM/EDS; FTIR analysis and discussion; pore size distribution analysis; TGA analyses; solid-state NMR spectra and calibration curve used for quantification of CO_2 uptake (PDF)

■ AUTHOR INFORMATION

Corresponding Authors

Mirtha A. O. Lourenço − *CICECO—Instituto de Materiais de Aveiro, Departamento de Química, Universidade de Aveiro, Campus Universitário de Santiago, 3810-193 Aveiro, Portugal;* orcid.org/0000-0003-0260-3422; Email: mirtha@ua.pt

Ildefonso Marin-Montesinos − *CICECO—Instituto de Materiais de Aveiro, Departamento de Química, Universidade de Aveiro, Campus Universitário de Santiago, 3810-193 Aveiro, Portugal;* orcid.org/0000-0002-4206-2643; Email: imarin@ua.pt

Luís Mafra − *CICECO—Instituto de Materiais de Aveiro, Departamento de Química, Universidade de Aveiro, Campus Universitário de Santiago, 3810-193 Aveiro, Portugal;* orcid.org/0000-0003-1028-8354; Email: lmafra@ua.pt

Authors

Daniel Pereira − *CICECO—Instituto de Materiais de Aveiro, Departamento de Química, Universidade de Aveiro, Campus Universitário de Santiago, 3810-193 Aveiro, Portugal;* orcid.org/0000-0001-7329-2516

Marina Ilkaeva − *CICECO—Instituto de Materiais de Aveiro, Departamento de Química, Universidade de Aveiro, Campus Universitário de Santiago, 3810-193 Aveiro, Portugal; Department of Chemical and Environmental Engineering, University of Oviedo, 33006 Oviedo, Spain;* orcid.org/0000-0001-9834-7042

Francisco Vicente − *CICECO—Instituto de Materiais de Aveiro, Departamento de Química, Universidade de Aveiro, Campus Universitário de Santiago, 3810-193 Aveiro, Portugal*

Ricardo Vieira − *CICECO—Instituto de Materiais de Aveiro, Departamento de Química, Universidade de Aveiro, Campus Universitário de Santiago, 3810-193 Aveiro, Portugal*

Mariana Sardo − *CICECO—Instituto de Materiais de Aveiro, Departamento de Química, Universidade de Aveiro, Campus Universitário de Santiago, 3810-193 Aveiro, Portugal;* orcid.org/0000-0003-3208-4387

Armando Silvestre − *CICECO—Instituto de Materiais de Aveiro, Departamento de Química, Universidade de Aveiro, Campus Universitário de Santiago, 3810-193 Aveiro, Portugal*

Complete contact information is available at:

https://doi.org/10.1021/acsomega.3c09423
ACS Omega 2024, 9, 17956−17965

https://pubs.acs.org/10.1021/acsomega.3c09423

Notes

The authors declare no competing financial interest.

■ ACKNOWLEDGMENTS

This work was developed within the scope of project CICECO-Aveiro Institute of Materials, UIDB/50011/2020, (DOI: 10.54499/UIDB/50011/2020), UIDP/50011/2020 (DOI: 10.54499/UIDP/50011/2020) & LA/P/0006/2020 (DOI: 10.54499/ LA/P/0006/2020), financed by national funds through the FCT/MEC (PIDDAC). We also acknowledge funding from project PTDC/QUI-QFI/28747/2017 (GAS2MAT-DNPSENS-POCI-01-0145-FEDER-028), financed through FCT/MEC and co-financed by FEDER under the PT2020 Partnership Agreement. The NMR spectrometers are part of the National NMR Network (PTNMR) and are partially supported by Infrastructure Project 022161 (co-financed by FEDER through COMPETE 2020, POCI and PORL and FCT through PIDDAC). This work has received funding from the European Research Council (ERC) under the European Union's Horizon 2020 research and innovation program (Grant Agreement 865974). FCT is also acknowledged by D.P. for a Ph.D. Studentship (UI/BD/151048/2021), M.I., R.V., M.A.O.L., and M.S. for Researcher positions (CEECIND/00546/2018, CEECIND/02127/2017, CEECIND/01158/2021 (DOI: 10.54499/2021.01158.CEECIND/CP1659/CT0022) and CEECIND/00056/2020 respectively (DOI 10.54499/2020.00056.CEECIND/CP1589/CT0005)). M.I. acknowledges Spanish Ministry of Science, Innovation, and Universities for the "Beatriz Galindo" Scholarship (MU-23-BG22/00145). M.A.O.L further acknowledges the funding from the European Union's Horizon 2020 research and innovation program (PF Grant Agreement 101090287).

■ REFERENCES

(1) Friedlingstein, P.; Jones, M. W.; O'Sullivan, M.; Andrew, R. M.; Bakker, D. C. E.; Hauck, J.; Le Quéré, C.; Peters, G. P.; Peters, W.; Pongratz, J.; Sitch, S.; Canadell, J. G.; Ciais, P.; Jackson, R. B.; Alin, S. R.; Anthoni, P.; Bates, N. R.; Becker, M.; Bellouin, N.; Bopp, L.; Chau, T. T. T.; Chevallier, F.; Chini, L. P.; Cronin, M.; Currie, K. I.; Decharme, B.; Djeutchouang, L. M.; Dou, X.; Evans, W.; Feely, R. A.; Feng, L.; Gasser, T.; Gilfillan, D.; Gkritzalis, T.; Grassi, G.; Gregor, L.; Gruber, N.; Gürses, Ö.; Harris, I.; Houghton, R. A.; Hurtt, G. C.; Iida, Y.; Ilyina, T.; Luijkx, I. T.; Jain, A.; Jones, S. D.; Kato, E.; Kennedy, D.; Klein Goldewijk, K.; Knauer, J.; Korsbakken, J. I.; Körtzinger, A.; Landschützer, P.; Lauvset, S. K.; Lefèvre, N.; Lienert, S.; Liu, J.; Marland, G.; McGuire, P. C.; Melton, J. R.; Munro, D. R.; Nabel, J. E. M. S.; Nakaoka, S.-I.; Niwa, Y.; Ono, T.; Pierrot, D.; Poulter, B.; Rehder, G.; Resplandy, L.; Robertson, E.; Rödenbeck, C.; Rosan, T. M.; Schwinger, J.; Schwingshackl, C.; Séférian, R.; Sutton, A. J.; Sweeney, C.; Tanhua, T.; Tans, P. P.; Tian, H.; Tilbrook, B.; Tubiello, F.; van der Werf, G. R.; Vuichard, N.; Wada, C.; Wanninkhof, R.; Watson, A. J.; Willis, D.; Wiltshire, A. J.; Yuan, W.; Yue, C.; Yue, X.; Zaehle, S.; Zeng, J. Global Carbon Budget 2021. *Earth Syst. Sci. Data* **2022**, *14*, 1917−2005.

(2) Chalmers, H.; Gibbins, J. Carbon capture and storage: The ten year challenge. *Proc. Inst. Mech. Eng., Part C* **2010**, *224*, 505−518.

(3) Wilberforce, T.; Baroutaji, A.; Soudan, B.; Al-Alami, A. H.; Olabi, A. G. Outlook of carbon capture technology and challenges. *Sci. Total Environ.* **2019**, *657*, 56−72.

(4) Bernin, D.; Hedin, N. Perspectives on NMR studies of CO2 adsorption. *Curr. Opin. Colloid Interface Sci.* **2018**, *33*, 53−62.

(5) Lee, S.-Y.; Park, S.-J. A review on solid adsorbents for carbon dioxide capture. *J. Ind. Eng. Chem.* **2015**, *23*, 1−11.

(6) Patel, H. A.; Byun, J.; Yavuz, C. T. Carbon Dioxide Capture Adsorbents: Chemistry and Methods. *ChemSusChem* **2017**, *10*, 1303−1317.

(7) Wang, J.; Huang, L.; Yang, R.; Zhang, Z.; Wu, J.; Gao, Y.; Wang, Q.; O'Hare, D.; Zhong, Z. Recent advances in solid sorbents for CO2 capture and new development trends. *Energy Environ. Sci.* **2014**, *7*, 3478−3518.

(8) Pereira, D.; Fonseca, R.; Marin-Montesinos, I.; Sardo, M.; Mafra, L. Understanding CO2 adsorption mechanisms in porous adsorbents: A solid-state NMR survey. *Curr. Opin. Colloid Interface Sci.* **2023**, *64*, No. 101690.

(9) Kolle, J. M.; Fayaz, M.; Sayari, A. Understanding the Effect of Water on CO2 Adsorption. *Chem. Rev.* **2021**, *121*, 7280−7345.

(10) Pardakhti, M.; Jafari, T.; Tobin, Z.; Dutta, B.; Moharreri, E.; Shemshaki, N. S.; Suib, S.; Srivastava, R. Trends in Solid Adsorbent Materials Development for CO2 Capture. *ACS Appl. Mater. Interfaces* **2019**, *11*, 34533−34559.

(11) Lippe, M.; Lewandowski, I.; Unseld, R.; Pucher, J.; Bräutigam, K.-R. *The Origin of Biomass—Bioeconomy for Beginners*; Pietzsch, J., Ed.; Springer: Berlin, Heidelberg, 2020; pp 11−66.

(12) European Commission. The Circular Economy and the Bioeconomy, 2018. https://circulareconomy.europa.eu/platform/sites/default/files/the_circular_economy_and_the_bioeconomy_-_partners_in_sustainabilitythal18009enn.pdf.

(13) Sharma, S.; Kaur, N.; Kaur, R.; Kaur, R. A review on valorization of chitinous waste. *J. Polym. Res.* **2021**, *28*, 406.

(14) Qaroush, A. K.; Alshamaly, H. S.; Alazzeh, S. S.; Abeskhron, R. H.; Assaf, K. I.; Eftaiha, A. F. Inedible saccharides: a platform for CO2 capturing. *Chem. Sci.* **2018**, *9*, 1088−1100.

(15) Nasri, N. S.; Hamza, U. D.; Ismail, S. N.; Ahmed, M. M.; Mohsin, R. Assessment of porous carbons derived from sustainable palm solid waste for carbon dioxide capture. *J. Cleaner Prod.* **2014**, *71*, 148−157.

(16) Hao, W.; Björnerbäck, F.; Trushkina, Y.; Oregui Bengoechea, M.; Salazar-Alvarez, G.; Barth, T.; Hedin, N. High-Performance Magnetic Activated Carbon from Solid Waste from Lignin Conversion Processes. 1. Their Use As Adsorbents for CO2. *ACS Sustainable Chem. Eng.* **2017**, *5*, 3087−3095.

(17) Ferrera-Lorenzo, N.; Fuente, E.; Suárez-Ruiz, I.; Ruiz, B. Sustainable activated carbons of macroalgae waste from the Agar−Agar industry. Prospects as adsorbent for gas storage at high pressures. *Chem. Eng. J.* **2014**, *250*, 128−136.

(18) Guardia, L.; Suárez, L.; Querejeta, N.; Pevida, C.; Centeno, T. A. Winery wastes as precursors of sustainable porous carbons for environmental applications. *J. Cleaner Prod.* **2018**, *193*, 614−624.

(19) Atta-Obeng, E.; Dawson-Andoh, B.; Felton, E.; Dahle, G. Carbon Dioxide Capture Using Amine Functionalized Hydrothermal Carbons from Technical Lignin. *Waste Biomass Valorization* **2019**, *10*, 2725−2731.

(20) Guo, X.; Zhang, G.; Wu, C.; Liu, J.; Li, G.; Zhao, Y.; Wang, Y.; Xu, Y. A cost-effective synthesis of heteroatom-doped porous carbon by sulfur-containing waste liquid treatment: As a promising adsorbent for CO2 capture. *J. Environ. Chem. Eng.* **2021**, *9*, No. 105165.

(21) Mumtaz, H.; Farhan, M.; Amjad, M.; Riaz, F.; Kazim, A. H.; Sultan, M.; Farooq, M.; Mujtaba, M. A.; Hussain, I.; Imran, M.; Anwar, S.; El-Sherbeeny, A. M.; Siddique, F. A.; Armaković, S.; Ali, Q.; Chaudhry, I. A.; Pettinau, A. Biomass waste utilization for adsorbent preparation in CO2 capture and sustainable environment applications. *Sustain. Energy Technol. Assessments* **2021**, *46*, No. 101288.

(22) Nguyen, H. N.; Nguyen, P. L. T.; Tran, V. B. Zero-waste biomass gasification: Use of residues after gasification of bagasse pellets as CO2 adsorbents. *Therm. Sci. Eng. Prog.* **2021**, *26*, No. 101080.

(23) Vazhayal, L.; Wilson, P.; Prabhakaran, K. Utilization of waste aquatic weeds for the sustainable production of nitrogen doped

nanoporous carbon for CO2 capture. *Mater. Today Proc.* **2022**, *52*, 2315−2321.
(24) Dissanayake, P. D.; You, S.; Igalavithana, A. D.; Xia, Y.; Bhatnagar, A.; Gupta, S.; Kua, H. W.; Kim, S.; Kwon, J.-H.; Tsang, D. C. W.; Ok, Y. S. Biochar-based adsorbents for carbon dioxide capture: A critical review. *Renewable Sustainable Energy Rev.* **2020**, *119*, No. 109582.
(25) Singh, G.; Lakhi, K. S.; Sil, S.; Bhosale, S. V.; Kim, I.; Albahily, K.; Vinu, A. Biomass derived porous carbon for CO2 capture. *Carbon* **2019**, *148*, 164−186.
(26) Xu, S.; Zhou, C.; Fang, H.; Zhu, W.; Shi, J.; Liu, G. Synthesis of ordered mesoporous silica from biomass ash and its application in CO2 adsorption. *Environ. Res.* **2023**, *231*, No. 116070.
(27) Khadir, A.; Negarestani, M.; Ghiasinejad, H. Low-cost sisal fibers/polypyrrole/polyaniline biosorbent for sequestration of reactive orange 5 from aqueous solutions. *J. Environ. Chem. Eng.* **2020**, *8*, No. 103956.
(28) Adigun, O. A.; Oninla, V. O.; Babarinde, N. A. A.; Oyedotun, K. O.; Manyala, N. Characterization of sugarcane leaf-biomass and investigation of its efficiency in removing Nickel(II), Chromium(III) and Cobalt(II) ions from polluted water. *Surf. Interfaces.* **2020**, *20*, No. 100621.
(29) Neville, A. C. *Introduction BT—Biology of the Arthropod Cuticle*; Springer: Berlin, Heidelberg, 1975; pp 1−6.
(30) Hu, X.; Liu, L.; Luo, X.; Xiao, G.; Shiko, E.; Zhang, R.; Fan, X.; Zhou, Y.; Liu, Y.; Zeng, Z.; Li, C. A review of N-functionalized solid adsorbents for post-combustion CO2 capture. *Appl. Energy* **2020**, *260*, No. 114244.
(31) Gu, C.; Liu, Y.; Wang, W.; Liu, J.; Hu, J. Effects of functional groups for CO2 capture using metal organic frameworks. *Front. Chem. Sci. Eng.* **2021**, *15*, 437−449.
(32) Lim, G.; Lee, K. B.; Ham, H. C. Effect of N-Containing Functional Groups on CO2 Adsorption of Carbonaceous Materials: A Density Functional Theory Approach. *J. Phys. Chem. C* **2016**, *120*, 8087−8095.
(33) Nisticò, R. Aquatic-Derived Biomaterials for a Sustainable Future: A European Opportunity. *Resources* **2017**, *6*, No. 65.
(34) Iftekhar Shams, M.; Nogi, M.; Berglund, L. A.; Yano, H. The transparent crab: preparation and nanostructural implications for bioinspired optically transparent nanocomposites. *Soft Matter* **2012**, *8*, 1369−1373.
(35) Jeon, D. J.; Yeom, S. H. Recycling wasted biomaterial, crab shells, as an adsorbent for the removal of high concentration of phosphate. *Bioresour. Technol.* **2009**, *100*, 2646−2649.
(36) Suryawanshi, N.; Jujjavarapu, S. E.; Ayothiraman, S. Marine shell industrial wastes—an abundant source of chitin and its derivatives: constituents, pretreatment, fermentation, and pleiotropic applications-a revisit. *Int. J. Environ. Sci. Technol.* **2019**, *16*, 3877−3898.
(37) Ifuku, S. Chitin and Chitosan Nanofibers: Preparation and Chemical Modifications. *Molecules* **2014**, *19*, 18367−18380.
(38) Nekvapil, F.; Aluas, M.; Barbu-Tudoran, L.; Suciu, M.; Bortnic, R.-A.; Glamuzina, B.; Pinzaru, S. C. From Blue Bioeconomy toward Circular Economy through High-Sensitivity Analytical Research on Waste Blue Crab Shells. *ACS Sustainable Chem. Eng.* **2019**, *7*, 16820−16827.
(39) Gbenebor, O. P.; Adeosun, S. O.; Lawal, G. I.; Jun, S. Role of CaCO3 in the physicochemical properties of crustacean-sourced structural polysaccharides. *Mater. Chem. Phys.* **2016**, *184*, 203−209.
(40) Jang, M.-K.; Kong, B.-G.; Jeong, Y.-I.; Lee, C. H.; Nah, J.-W. Physicochemical characterization of α-chitin, β-chitin, and γ-chitin separated from natural resources. *J. Polym. Sci., Part A: Polym. Chem.* **2004**, *42*, 3423−3432.
(41) Goodrich, J. D.; Winter, W. T. α-Chitin Nanocrystals Prepared from Shrimp Shells and Their Specific Surface Area Measurement. *Biomacromolecules.* **2007**, *8*, 252−257.
(42) Zhao, D.; Huang, W.-C.; Guo, N.; Zhang, S.; Xue, C.; Mao, X. Two-Step Separation of Chitin from Shrimp Shells Using Citric Acid and Deep Eutectic Solvents with the Assistance of Microwave. *Polymers* **2019**, *11*, No. 409.
(43) Hassainia, A.; Satha, H.; Boufi, S. Chitin from Agaricus bisporus: Extraction and characterization. *Int. J. Biol. Macromol.* **2018**, *117*, 1334−1342.
(44) Rahman, M. A.; Halfar, J. First evidence of chitin in calcified coralline algae: new insights into the calcification process of Clathromorphum compactum. *Sci. Rep.* **2014**, *4*, No. 6162.
(45) Gbenebor, O. P.; Adeosun, S. O.; Lawal, G. I.; Jun, S.; Olaleye, S. A. Acetylation, crystalline and morphological properties of structural polysaccharide from shrimp exoskeleton. *Eng. Sci. Technol. Int. J.* **2017**, *20*, 1155−1165.
(46) Synowiecki, J.; Al-Khateeb, N. A. Production, Properties, and Some New Applications of Chitin and Its Derivatives. *Crit. Rev. Food Sci. Nutr.* **2003**, *43*, 145−171.
(47) Chang, J.; Shen, Z.; Hu, X.; Schulman, E.; Cui, C.; Guo, Q.; Tian, H. Adsorption of Tetracycline by Shrimp Shell Waste from Aqueous Solutions: Adsorption Isotherm, Kinetics Modeling, and Mechanism. *ACS Omega* **2020**, *5*, 3467−3477.
(48) Pessoa, M. E. A.; de Sousa, K. S.; Clericuzi, G. Z.; Ferreira, A. L.; Soares, M. C.; Neto, J. C. Adsorption of Reactive Dye onto Uçá Crab Shell (Ucides cordatus): Scale-Up and Comparative Studies. *Energies* **2021**, *14*, No. 5876.
(49) Hunt, S.; Huckerby, T. N. A comparative study of molluscan and crustacean chitin proteoglycans by carbon-13 NMR spectroscopy. Identification of carbohydrate and amino acid contributions and the determination of amino acid chemical shifts in anhydrous formic acid. *Comp. Biochem. Physiol., Part B: Biochem. Mol. Biol.* **1987**, *88*, 1107−1116.
(50) Kameda, T.; Miyazawa, M.; Ono, H.; Yoshida, M. Hydrogen Bonding Structure and Stability of α-Chitin Studied by 13C Solid-State NMR. *Macromol. Biosci.* **2005**, *5*, 103−106.
(51) Vieira, R.; Marin-Montesinos, I.; Pereira, J.; Fonseca, R.; Ilkaeva, M.; Sardo, M.; Mafra, L. "Hidden" CO2 in Amine-Modified Porous Silicas Enables Full Quantitative NMR Identification of Physi- and Chemisorbed CO2 Species. *J. Phys. Chem. C* **2021**, *125*, No. 14797.
(52) Witherspoon, V. J.; Xu, J.; Reimer, J. A. Solid-State NMR Investigations of Carbon Dioxide Gas in Metal-Organic Frameworks: Insights into Molecular Motion and Adsorptive Behavior. *Chem. Rev.* **2018**, *118*, 10033−10048.
(53) Danaci, D.; Bui, M.; Mac Dowell, N.; Petit, C. Exploring the limits of adsorption-based CO2 capture using MOFs with PVSA—from molecular design to process economics. *Mol. Syst. Des. Eng.* **2020**, *5*, 212−231.

https://doi.org/10.1021/acsomega.3c09423
ACS Omega 2024, 9, 17956−17965